

Article

Understanding the Catalytic Deactivation upon Hydrothermal Aging at 850 °C of WO₃/Fe-Cu-ZSM-5 Catalyst for Selective Catalytic Reduction of NO by NH₃

Houda Jouini ^{1,2,*} , Alessandra de Marcos-Galán ³ , Imène Mejri ^{1,2}, Rahma Bensouilah ¹, Mourad Mhamdi ^{1,2}, Teresa Blasco ³  and Gérard Delahay ⁴ 

¹ LR01ES08 Laboratoire de Chimie des Matériaux et Catalyse, Faculté des Sciences de Tunis, Université de Tunis El Manar, Tunis 2092, Tunisia

² Institut Supérieur des Technologies Médicales de Tunis, Université de Tunis El Manar, Tunis 1006, Tunisia

³ Instituto de Tecnología Química, Universitat Politècnica de València—Consejo Superior de Investigaciones Científicas (UPV-CSIC), Avda. de los Naranjos s/n, 46022 Valencia, Spain

⁴ Institut Charles Gerhardt Montpellier (ICGM), Université de Montpellier, CNRS, ENSCM, 34293 Montpellier, France

* Correspondence: houda.jouini@fst.utm.tn; Tel.: +216-99-92-56-55

Abstract: A WO₃/Fe-Cu-ZSM-5 catalyst was prepared using the solid state ion exchange method (SSIE) and its performance for the Selective Catalytic Reduction of NO with NH₃ (NH₃-SCR of NO) was investigated. The study shows that the tungsten addition can slightly improve the high temperature catalytic activity of Fe-Cu-ZSM-5. The influence of hydrothermal aging at 850 °C for 5 h on the structural and textural properties of WO₃/Fe-Cu-ZSM-5 was also studied in this paper. The XRD and FE-SEM measurements did not indicate a breakdown of the zeolite structure upon steam treatment for both aged catalysts. The aged W-base catalyst demonstrates a lower deactivation and better catalytic activity for NO reduction than the bimetallic catalyst after hydrothermal aging despite the lower acidic properties as shown by FTIR-Pyr spectroscopy owing to the presence of tungsten oxide crystallites. The “severe” stage of aging occurring in the absence of W led to the formation of copper oxide agglomerates detected using STEM and H₂-TPR techniques being responsible for the deterioration of SCR activity of the aged Fe-Cu-ZSM-5.

Keywords: tungsten; SSIE; SCR; aging; ZSM-5



Citation: Jouini, H.; de Marcos-Galán, A.; Mejri, I.; Bensouilah, R.; Mhamdi, M.; Blasco, T.; Delahay, G.

Understanding the Catalytic Deactivation upon Hydrothermal Aging at 850 °C of WO₃/Fe-Cu-ZSM-5 Catalyst for Selective Catalytic Reduction of NO by NH₃. *Inorganics* **2022**, *10*, 180. <https://doi.org/10.3390/inorganics10110180>

Academic Editors: Tzia Ming Onn and Raymond J. Gorte

Received: 19 September 2022

Accepted: 22 October 2022

Published: 25 October 2022

Publisher's Note: MDPI stays neutral with regard to jurisdictional claims in published maps and institutional affiliations.



Copyright: © 2022 by the authors. Licensee MDPI, Basel, Switzerland. This article is an open access article distributed under the terms and conditions of the Creative Commons Attribution (CC BY) license (<https://creativecommons.org/licenses/by/4.0/>).

1. Introduction

Selective Catalytic Reduction (SCR) is a chemical process that reduces nitrogen oxides produced during the combustion process of hydrocarbon fuels. Its main role is to limit pollution in order to meet anti-pollution standards. Nitrogen oxide (NO) is a colorless gas with the ability to oxidize in air forming nitrogen dioxide (NO₂). In high concentrations, it causes nervous system paralysis. NO₂ is a brown colored gas with a pungent odor. Combined with sunlight and hydrocarbons, NO₂ forms smog. Nitrogen oxides (NO_x) are reduced by the SCR process in the exhaust gases containing oxygen. The exhaust gases, treated with a reactive solution of ammonia/urea, pass through the honeycomb-structured converters of fine cells, reducing nitrogen oxides to water and nitrogen. On vehicles with diesel engines, the SCR system is located on the exhaust, mounted downstream of an economizer and/or air heater and, in some cases, downstream of a dust collector. The optimum temperature range for this system is 300–400 °C and the reaction is slightly exothermic [1]. In some applications, gas reheating is used to maintain an optimum temperature for the catalyst bed. Most of the nitrogen compounds contained in exhaust gases are in the form of NO. The main SCR reaction (Standard SCR) is considered to be the following [2]:



Nevertheless, N_2O , a greenhouse gas, may be also produced from direct ammonia oxidation and ammonium nitrate decomposition during the SCR process.

Catalysts are based on a number of materials, the most popular being metal oxides and metal-exchanged zeolites [1,2], and are typically located in units between the economizer and the preheater. The catalyst unit can adopt the form of a plate, honeycomb, grid cylinder, or pellet reactor mounted in a carbon steel housing. They must be robust enough to withstand thermal cycling, sulfur, and halogen attack/poisoning and be able to resist the ash clogging.

Owing to its unique pore structure, strong acidity, larger surface area, and excellent thermal stability [3], ZSM-5 (MFI) zeolite has been widely utilized as the catalytic support material for the SCR process [4]. The SCR of NO over Cu and Fe supported on ZSM-5 has been extensively studied [5–8]. The bimetallic Fe-Cu catalyst showed higher activity than monometallic catalysts, thanks to the synergetic effect between the two metals [5].

W-based ZSM-5 catalysts are broadly investigated for environmental applications. The W-ZSM-5 catalyst showed remarkable hydrothermal stability and oxidation resistance in catalytic oxidation and catalytic cracking processes [9,10]. The study of W-ZSM-5 system by Chen et al. revealed that the introduction of tungsten improved the stability of the Si-O-Al structure through the elimination of the non-skeleton Al and regulated the acidity of ZSM-5 during the cracking of 1-hexene to propene reaction [11]. Tungsten showed in the SCR of NO in the presence of acetylene promoting effects on HZSM-5 support as reported by Wang et al. [12]. The W(6%)/HZSM-5 catalyst at 350 °C converted about 90% of the NO into N_2 . The W incorporation was effective to accelerate the NO oxidation to NO_2 and enlarge the strong adsorption of NO_x on the catalyst surface and thus considerably enhance the C_2H_2 -SCR of the NO reaction. Liu and co-workers studied the high-temperature NH_3 -SCR of NO over an Fe-Ni-W catalyst. The main challenge in the catalytic performance at high temperatures was the complex side reaction of NH_3 oxidation, which was suppressed owing to multi-metal centers supported on ZSM-5 support [13].

In this paper, we attempt to modify the Fe-Cu-ZSM-5 catalyst with WO_3 to develop a more efficacious catalyst for NO reduction from diesel exhaust emissions through an NH_3 -SCR pathway. The behavior of the studied catalyst upon a process of high temperature aging assimilating the harsh conditions of diesel engines was also investigated thus targeting either marine or automotive applications [14,15].

2. Results

The elemental analysis of studied samples was carried out by ICP-OES, Table 1 summarizes the relative contents of the contents of Cu, Fe, and W expressed in wt.%. The examination of ICP results shows that the SSIE preparation method was effective to control the amount of metals exchanged with the zeolite support, which is in accordance with our previous studies [5,8].

Table 1. ICP-OES chemical analysis results.

Sample Label	Theoretical Composition	Fe (wt.%)	Cu (wt.%)	W (wt.%)
Fe-Cu-Z	Fe (2 wt.%) - Cu (1.5 wt.%)	1.83	1.40	-
W-Fe-Cu-Z	W (2 wt.%) - Fe (2 wt.%) - Cu (1.5 wt.%)	1.72	1.48	2.02

All fresh samples were found to be microporous in N_2 physisorption studies at 77 K, with BET surface areas (Table 2) ranging from 327 to 291 m^2/g , primarily dependent on the composition of each sample. There was a small reduction in the BET surface (11%) and micropore volume (58%) for the Fe-Cu-Zag sample as compared to the fresh sample. There was a reduction in micropores, which can be caused by Al removal from the zeolite framework and the hydrolysis of the Si-O-Al bonds. The dramatic aging-related decrease in pore size indicates that an agglomerated phase may have occluded the zeolite pores. The addition of W on the bimetallic catalyst also resulted in a slight reduction in the BET surface area (7%) and pore volume (25%). The W-doped sample has kept its S_{BET} and

doubled its micropore volume after hydrothermal treatment. In general, these material textural qualities ought to deteriorate. This outcome could be explained by either (1) the development of a new phase resulting in the generation of secondary pores or (2) the stability of the texture brought on by the presence of tungsten.

Table 2. N₂ physisorption at 77 K results.

Sample	S _{BET} ^a (m ² /g)	Micropore Volume ^b (cm ³ /g)	Pore Size ^c (Å)
Fe-Cu-Z	327	0.110	287.90
Fe-Cu-Zag	291	0.046	56.92
W-Fe-Cu-Z	304	0.063	69.94
W-Fe-Cu-Zag	306	0.122	29.45

^a calculated by BET method. ^b calculated by t-plot method. ^c calculated by BJH method.

According to the categorization of IUPAC [16], the nitrogen adsorption–desorption isotherm for fresh samples displayed the Type H3 loop as seen in Figure 1, but aged samples displayed the Type H4 loop, indicating the presence of mesoporosity created by the packing of zeolite nanocrystals [17]. Hysteresis loop thickness varies between the fresh and aged samples, suggesting that hydrothermal treatment alters the ZSM-5 pore shape. The Type H5 loop, on the other hand, is visible in the W-Fe-Cu-Zag sample and has a characteristic form that is connected to certain pore structures that contain both open and partially blocked mesopores (plugged structure) [16].

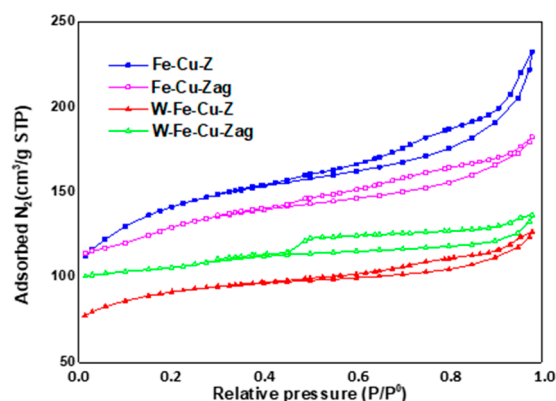


Figure 1. N₂ Adsorption–desorption isotherms of fresh and steamed Fe-Cu-Z and W-Fe-Cu-Z.

Fresh and aged samples were subjected to XRD measurements to look for any potential structural alterations. The investigated recorded XRD patterns (Figure 2) exhibit the typical MFI (Mobile-type Five) diffraction peaks of ZSM-5 (JCPDS #73-1138). Given the low metal content of the samples (0.5–2 wt.%), it was not surprising that the introduction of metals (Fe, Cu, and W) did not cause any discernible alterations in the ZSM-5 crystalline structure. No discernible metal oxide diffraction peaks were observed, indicating that the metal species were primarily in an amorphous state or were widely scattered within the zeolite structure [18,19].

XRD pattern of Fe-Cu-Zag showed a decrease in the peaks intensity with the absence of any extra-framework metal phase or any indication of possible amorphization. In the diffractogram of W-Fe-Cu-Zag (Figure 2b), four diffraction lines associated with crystalline WO₃ (JCPDS #01-089-4479) were detected at 2θ = 25.7 (012); 29.3 (211); 36.7 (103); and 38.7 (113).

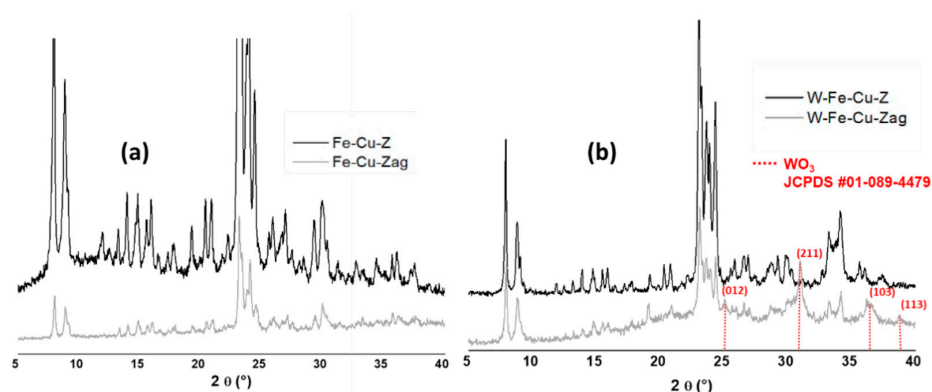


Figure 2. XRD diffractograms of fresh and aged (a) Fe-Cu-Z and (b) W-Fe-Cu-Z catalysts.

The studied catalysts were subjected to FE-SEM analysis and the recorded micrographs are shown in Figure 3. Well-crystallized zeolite particles with uneven localization, clear edges, good crystallization, and with an average length and width of 146 nm and 105 nm, respectively, were found in both fresh and aged samples. Thus, we demonstrate that the zeolite crystals of aged samples exhibit the same morphology of the fresh zeolite crystals supporting the findings of the DRX investigation.

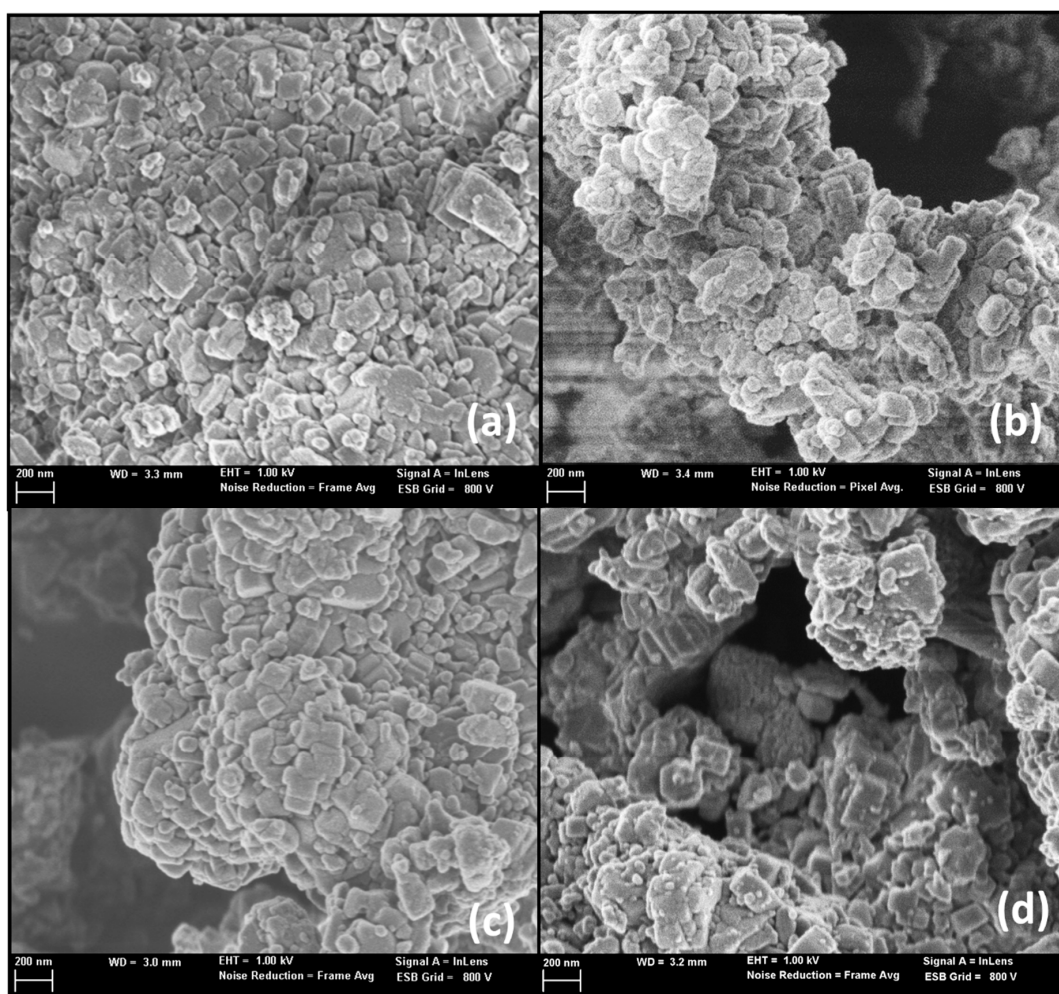


Figure 3. FE-SEM micrographs of (a) Fe-Cu-Z, (b) Fe-Cu-Zag, (c) W-Fe-Cu-Z, and (d) W-Fe-Cu-Zag catalysts.

Structure modifications upon W exchange and steam treatment were investigated using MAS ^{27}Al -NMR spectroscopy (Figure 4).

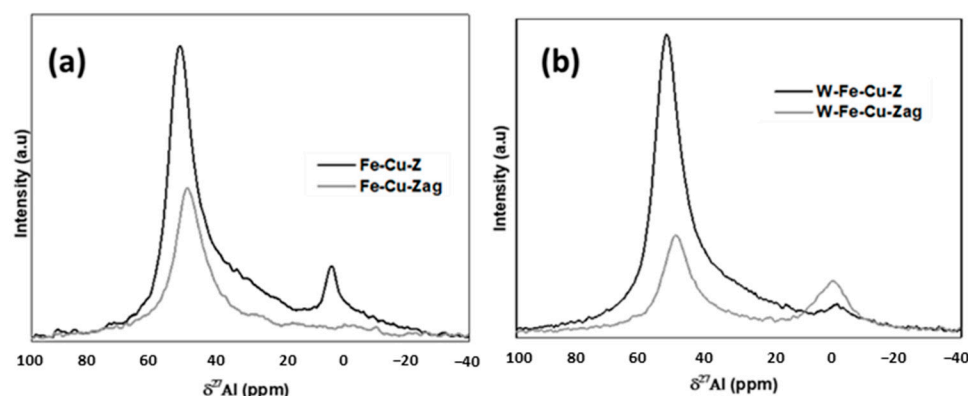


Figure 4. ^{27}Al NMR spectra of fresh and aged (a) Fe-Cu-Z and (b) W-Fe-Cu-Z.

After tungsten modification (Figure 4b), the resonance intensity at 55 ppm (framework Al, Td symmetry) rose, whereas the minor resonance at 0 ppm (extra-framework Al, Oh symmetry) disappeared. The existence of a tetrahedral W-O-Al structure was shown by the increase in peak intensity around 55 ppm [20], while the disappearance of the peak at 0 ppm illustrated that the exchanged W induced a hexahedral structure with extra-framework Al [21].

Both aged samples showed a decrease in the intensity of the peak around 55 ppm indicating that the aging has disrupted the coordination of framework Al species.

For Fe-Cu-Zag, the intensity of the EFAL peak decreased, indicating a reduction in the number of extra-framework Al species. The reason of this behavior is that some amounts of non-framework Al species in the main zeolite channels may be cleaned under heat treatment corresponding to a healing process, which smooths the zeolite channels [22]. This healing process would normally increase the pore volume of the catalyst. However, the opposite result is observed because of the important extent of the zeolite dealumination under such severe steaming conditions [22].

The spectra acquired from the ^{29}Si MAS NMR analysis of the analyzed materials were displayed in Figure 5. Resonances observed at about -113 ppm and -115 ppm (visible in the case of W-Fe-Cu-Zag sample) correspond to Si(4Si,0Al) sites [23]. The shoulder around -106 ppm arises from Si(3Si,1Al) sites: Si atoms with one neighboring Al atom [23]. All recorded spectra do not exhibit any band with chemical shifts underneath -100 ppm that might be ascribed to Si(2Al). This unequivocally demonstrates that Al-O-Si-O-Al sequences are missing from our samples [24].

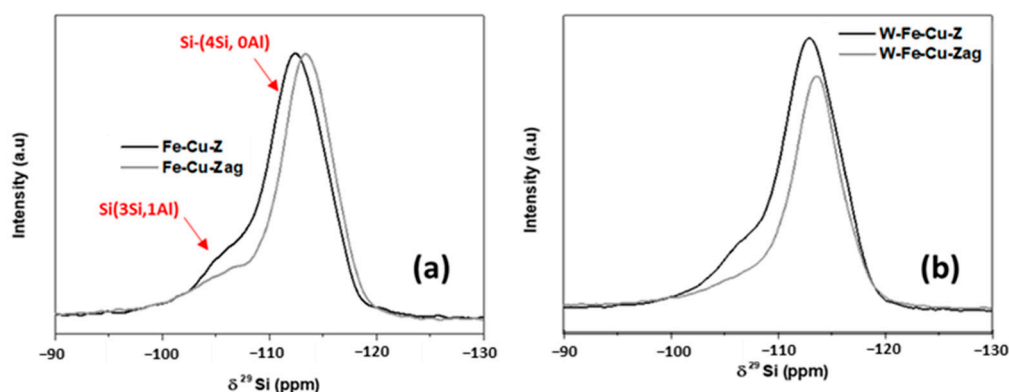


Figure 5. ^{29}Si NMR spectra of fresh and aged (a) Fe-Cu-Z and (b) W-Fe-Cu-Z.

The ^{29}Si NMR spectrum of W-Fe-Cu-Zag showed that the intensity of the resonance was at about -106 ppm, decreased to a good extent. This might occur as a portion of Si(1Al) was converted, showing that the impact of dealumination in the case of the trimetallic sample is more significant than for Fe-Cu-Zag. This finding is in line with the results of ^{27}Al MAS NMR showing that the amount of EFAL clearly increased in the case of W-Fe-Cu-Zag. The above results can be attributed to the weak interaction of W species with the framework Al of the support allowing a higher extraction of EFAL during steam treatment [24].

The investigated samples have been the subject of several STEM observations (Figure 6). The EDX reports of analyzed spectra recorded on the studied samples were provided in the “Supplementary Materials” section. By using EDX elemental analysis, the distributions of Fe, Cu, and W species were verified. The STEM image of the Fe-Cu-Z material (Figure 6a) only revealed a small number of large Fe nanocomposites (17–38 nm). Cu particles of a lower size were also detected (5 nm). Both iron and copper agglomerated significantly in the case of Fe-Cu-Zag (Figure 6b). The largest size of the copper particles, having a meaningful amount and rather homogeneous dispersion, is 11 nm.

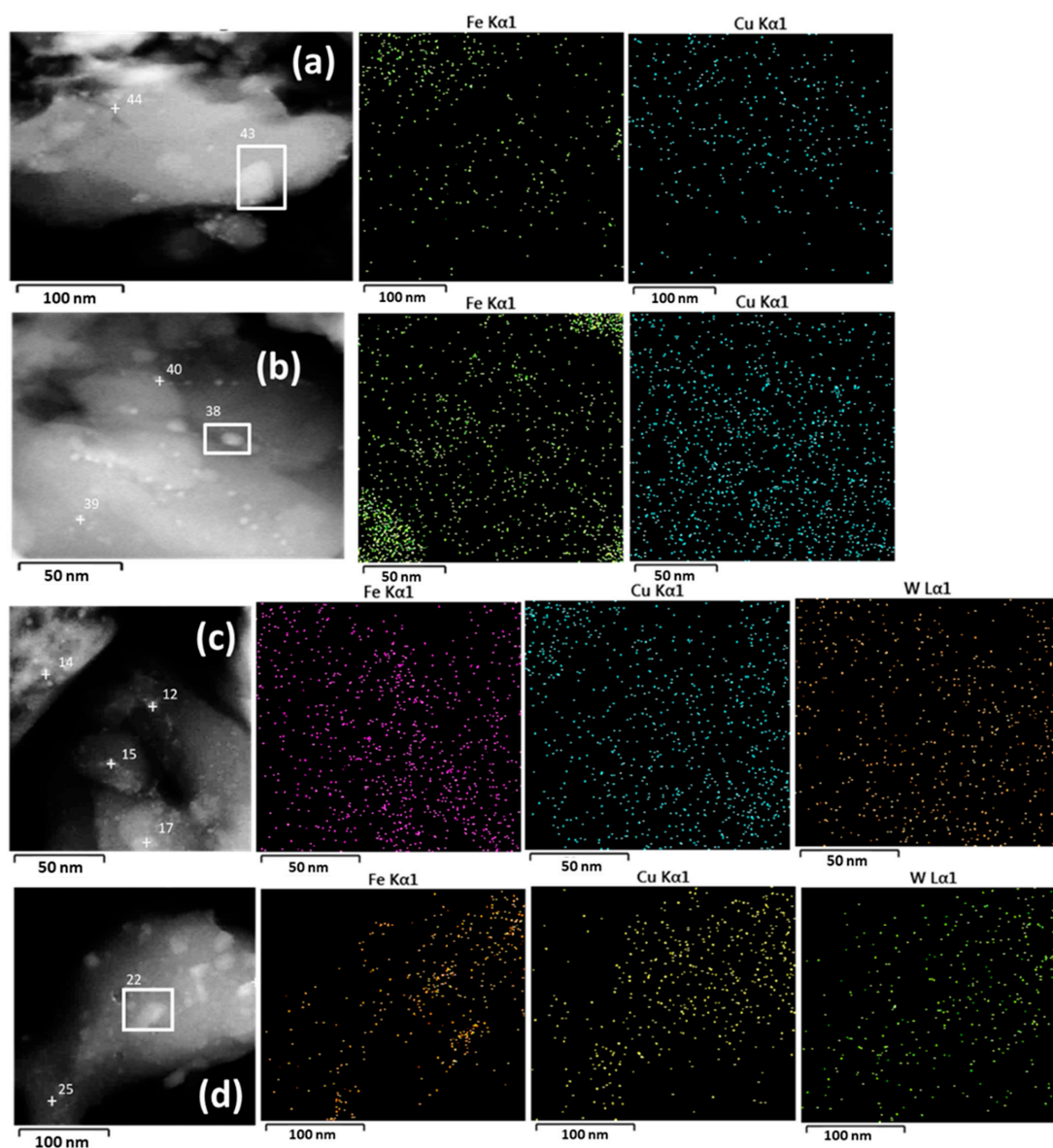


Figure 6. STEM micrographs and EDX mapping images of (a) Fe-Cu-Z, (b) Fe-Cu-Zag, (c) W-Fe-Cu-Z, and (d) W-Fe-Cu-Zag catalysts.

The inclusion of W helps to improve the dispersion of Fe and Cu species, according to the EDX mapping images of W-Fe-Cu-Z; highly dispersed W particles less than 2 nm in size have been detected. The aging treatment dramatically increased the amount of Fe agglomeration: Fe particles with sizes between 27 and 50 nm and W particles with an average size of about 9 nm were both observed.

To determine the local environment of transition metals, both untreated and aged samples were subjected to UV-Vis experiments. Reflectance data were used to calculate the Kubelka–Munk function and obtained spectra were provided in Figure 7. In order to resolve the sub-bands buried in the recorded spectra, the deconvolution method was used since the bands shape was not symmetric and not composed of a single band. Through the use of a Matlab technique, UV-vis spectra have been divided into three or four Gaussian components which have been assigned according to the literature in Table 3.

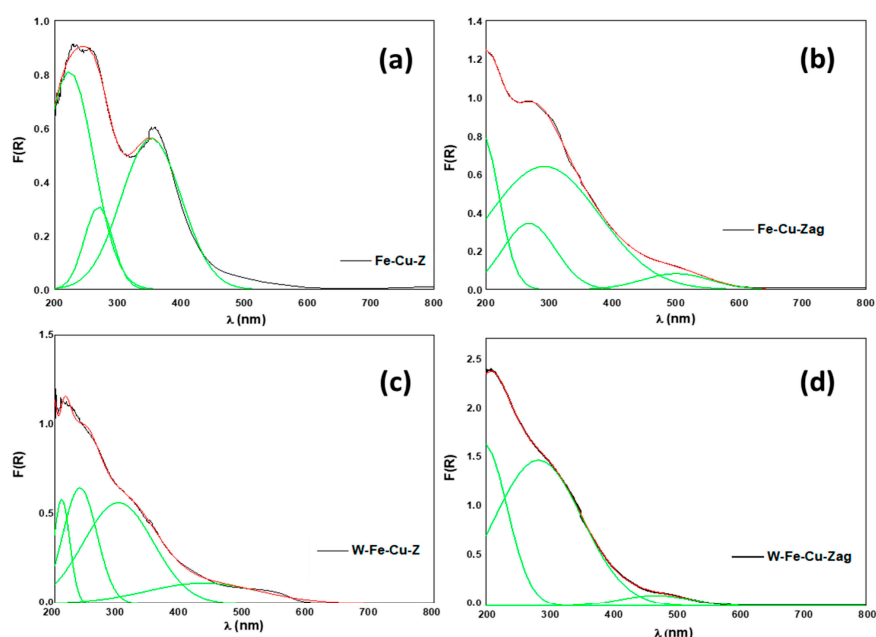


Figure 7. DRS UV-vis spectra of (a) Fe-Cu-Z, (b) Fe-Cu-Zag, (c) W-Fe-Cu-Z, and (d) W-Fe-Cu-Zag catalysts.

Table 3. Assignment of the different UV-Vis bands according to the literature.

Catalyst	λ (nm)	Attribution	Reference
Fe-Cu-Z (Figure 7a)	223	isolated mononuclear Fe ³⁺ (Td)	[25]
	271	isolated mononuclear Fe ³⁺ (Oh)	[25]
	353	oligomeric Fe ³⁺ _x O _y clusters	[25]
Fe-Cu-Zag (Figure 7b)	201	zeolite matrix	[26]
	265	isolated mononuclear Fe ³⁺ (Oh)	[25]
	292	isolated mononuclear Fe ³⁺ (Oh)	[25]
	501	Bulk CuO	[27]
W-Fe-Cu-Z (Figure 7c)	211	partially polymerized W(VI)/Surface WO ₃	[28,29]
	240	W species (low nuclearity)/tetrahedrally coordinated W (VI)	[11,29]
	301	oligomeric Fe ³⁺ _x O _y clusters	[25]
	435	Bulk WO ₃	[30]
W-Fe-Cu-Zag (Figure 7d)	198	MFI matrix	[26]
	284	isolated mononuclear Fe ³⁺ (Oh)	[25]
	478	Bulk WO ₃	[30]

The UV-vis results of the W-Fe-Cu-Z catalyst highlight that low nuclearity tungsten oxide species coexist with tungsten that has been incorporated into the framework. Those absorptions have disappeared after the hydrothermal treatment; the reported absorption band of bulk WO_3 has undergone a bathochromic shift as the nuclearity of tungsten entities increases upon steam treatment [29]. According to the high-angle XRD data and the observed variation of this band ascribed to bulk WO_3 , the crystalline WO_3 in W-Fe-Cu-Zag is mostly produced from amorphous tungsten oxide in the corresponding fresh sample. These findings concur with heat decomposition analyses of the W precursor (ammonium metatungstate), which indicate the production of an amorphous W phase that transforms into crystallized WO_3 upon heating at high temperatures [31].

The H_2 -TPR experiments were carried out to investigate the redox characteristics of the various examined catalysts. Presented in Figure 8 are H_2 -TPR profiles over the analyzed catalysts before and after steaming. It should be noted that there were no H_2 consumption peaks by unexchanged ZSM-5 in the test temperature range.

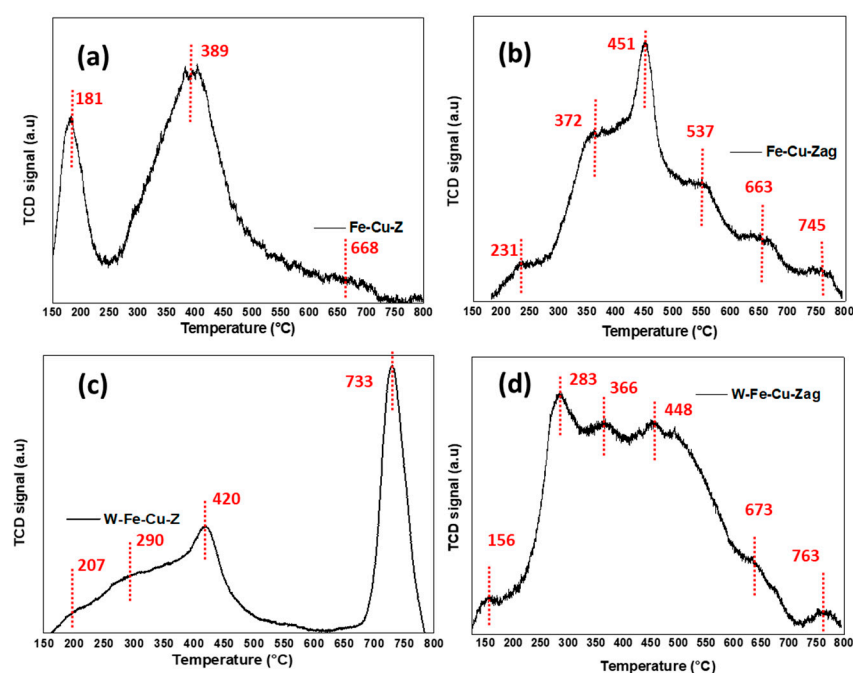


Figure 8. H_2 -TPR profiles of (a) Fe-Cu-Z, (b) Fe-Cu-Zag, (c) W-Fe-Cu-Z, and (d) W-Fe-Cu-Zag catalysts.

Previous studies [32,33] defined two fundamental reduction zones for the H_2 -TPR profile of Cu and Fe-based zeolite materials: peaks around 300–400 °C are ascribed to the reduction of Fe^{3+} and/or Fe_2O_3 to Fe^{2+} , whereas peaks above 450 °C correspond to the reduction of Fe^{2+} and/or FeO to Fe^0 .

Since copper species may be reduced at lower temperatures (200–400 °C) than iron species, they are more readily reducible. According to the literature [34–36], both active cupric species in ZSM-5 zeolite (Cu oxides and isolated Cu^{2+} located at exchange sites) are reduced by hydrogen at temperatures below 230 °C, while isolated Cu^{2+} at exchange sites are reduced at around 160–200 °C and CuO crystallites at 200–250 °C. The reduction above 330 °C is ascribed to the reduction of Cu^+ (formed from the reduction of Cu^{2+} and CuO) to Cu^0 .

The TPR profile of bulk WO_3 shows two peaks with maxima at around 750–800 °C and above 800 °C. These peaks can be ascribed, respectively, to the two stepwise reduction of WO_3 to W^0 : $\text{W}^{6+} \rightarrow \text{W}^{4+}$ and $\text{W}^{4+} \rightarrow \text{W}^0$ [37,38].

As shown in Figure 8b, upon aging at 850 °C, a reduction peak appears at 231 °C for Fe-Cu-Zag, which is assigned to CuO clusters. According to Cavataio et al. [35], the new

peaks appearing above 400 °C upon the aging treatment would arise from metal species that interact with destroyed zeolite and therefore are inactive for the SCR reaction in the presence of ammonia. Thus, Fe-Cu-Zag displayed a small H₂ consumption peak at 745 °C. Since this catalyst is W-free, this peak was found to arise from the reduction of CuAl₂O₄ species formed during the steam treatment [39]. ²⁷Al NMR showed a decrease in the amount of EFAL in the case of Fe-Cu-Zag, which consolidates the possibility of CuAl₂O₄. In the case of W-Fe-Cu-Zag (Figure 8d), the position of the reduction peaks attributed to Fe and Cu species shifted to a lower temperature compared to Fe-Cu-Zag, suggesting that the doping of W increased the reduction capacity of the aged catalyst. Therefore, the improved reduction property of this catalyst compared to bimetallic Fe-Cu-Zag was beneficial to the NH₃-SCR. The hydrothermally treated trimetallic catalyst showed a slight high temperature shift of the WO₃ reduction peak detected above 700 °C, this could be caused by the transfer of Cu from exchange sites to the surface or is thought to be an indicator of strong interactions between oxide species and the zeolite [36].

The acidity modification before and after steam treatment was checked for the prepared materials by the FTIR-Pyr technique. The recorded spectra at different evacuation temperatures (150, 250, 350, and 400 °C) were gathered in Figure 9. Using the molar extinction coefficients listed in the literature [40], the concentrations of Lewis and Brønsted acid sites (Table 4) were determined from the integrated areas of the FTIR-Pyr bands at 1450 and 1545 cm⁻¹, respectively.

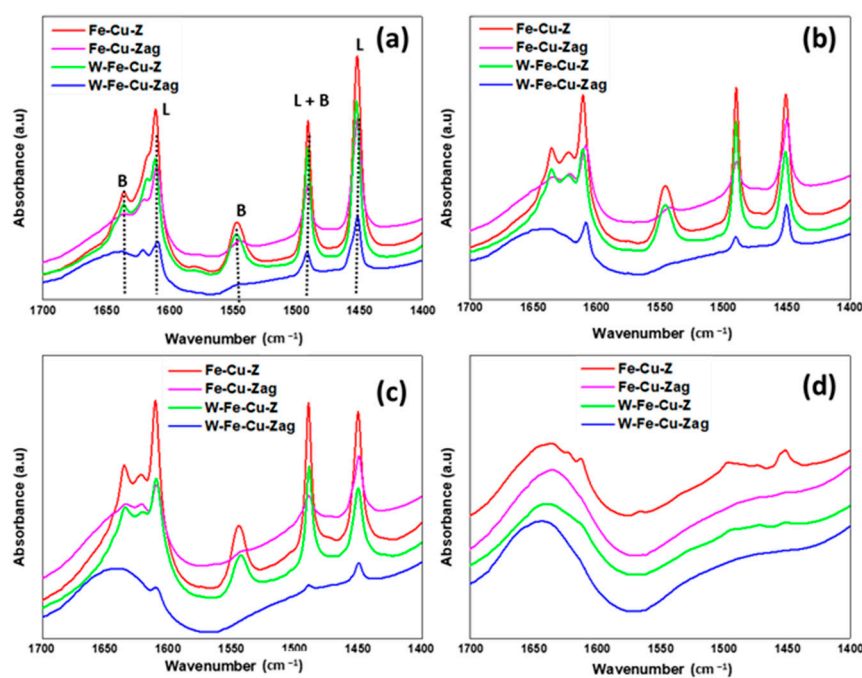


Figure 9. FTIR-Pyr spectra of fresh and aged catalysts degassed at (a) 150 °C, (b) 250 °C, (c) 350 °C, and (d) 400 °C.

Chemisorbed pyridine is recognized by the conventional set of stretching vibrations: (L) two bands at 1450 and 1610 cm⁻¹ assigned to coordinately bonded pyridine to Lewis acid sites; (B) two bands at 1545 and 1635 cm⁻¹ assigned to pyridinium cations PyH⁺ (pyridine protonated by Brønsted acid sites); and (B + L) the superposition of signals of Lewis and Brønsted adsorbed species at approximately 1490 cm⁻¹ [24].

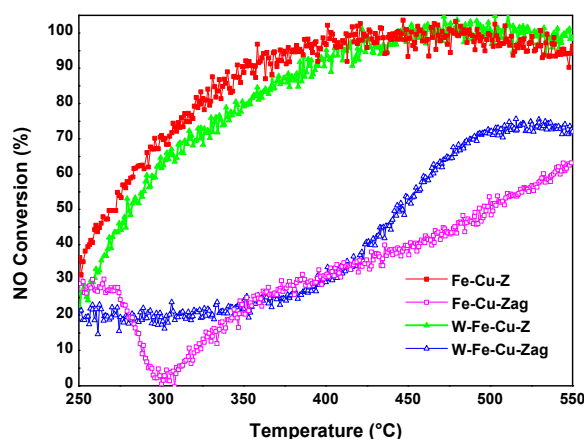
The incorporation of W onto the Fe-Cu-Z material caused a decrease in both B and L peaks, this was predicted since the exchanged tungsten species replaced the acid sites. The interaction between W and the C-H bond in the pyridine could be the cause of the decrease in the peak at 1490 cm⁻¹ arising from the (B + L) acid sites [41].

Table 4. FTIR-Pyr quantitative study of acid centers.

Sample	Temperature (°C)	Acid Centers ($\mu\text{mol Py/gr}$)			
		Brönsted	Lewis	B350/B150	L350/L150
Fe-Cu-Z	150	526	999	0.67	0.35
	250	495	499		
	350	356	353		
Fe-Cu-Zag	150	86	341	0.24	0.27
	250	55	164		
	350	21	92		
W-Fe-Cu-Z	150	380	715	0.70	0.31
	250	378	307		
	350	265	224		
W-Fe-Cu-Zag	150	34	185	0.051	0.20
	250	16	120		
	350	2	38		

After outgassing at 250 °C, the intensities of all FTIR-Pyr bands were progressively reduced, those of aged samples and especially W-Fe-Cu-Zag were obviously more affected. After outgassing at 400 °C, all detected FTIR-Pyr bands vanished for both steamed samples. Table 4 shows that the ratio between the Lewis acid sites (L350/L150) was maintained for W-Fe-Cu-Zag compared to the bimetallic sample, probably owing to the presence of tungsten oxide species in a tetrahedral coordination, detected previously from UV-vis and H₂-TPR techniques, presenting the characteristics of Lewis acid centers [41]. Meanwhile, the B350/B150 ratio has considerably decreased upon aging demonstrating that after the hydrothermal treatment of the trimetallic catalyst, the loss of the Brönsted sites is greater than the loss of Lewis sites. This finding confirms the NMR results showing that dealumination in the case of trimetallic sample was more significant.

Over 95% of the NO was converted using a fresh Fe-Cu-Z catalyst at temperatures between 365 and 590 °C (Figure 10). However, the NH₃ oxidation caused a decrease in NO conversion at temperatures above 500 °C. The supply of NH₃ for NO reduction is constrained by this side reaction, which limits the conversion of nitrogen oxide at high temperatures. The conversion profile of a fresh W-Fe-Cu-Z catalyst remained lower than that of the bimetallic catalyst until about 450 °C and the NO conversion was recorded as 95% at 410 °C. The catalytic results show that tungsten limits the ammonia oxidation capacity to NO of the Fe-Cu-ZSM-5 catalyst to a good extent. This finding is consistent with those of Väliheikki et al., who found that the substantial ammonia-inhibiting adsorption led to limited NH₃ conversion in W-based ZSM-5 catalyst [42].

**Figure 10.** NO conversion over fresh and aged catalysts.

After steam treatment, a considerable deactivation is seen for aged samples across the entire temperature window and this was more considerable for the bimetallic Fe-Cu-Z catalyst. The starting NO conversion of the Fe-Cu-Zag catalysts was 30% the same as that of the fresh sample and then surprisingly diminished to become inactive at around 300 °C. Above this point, a significant improvement in the conversion is seen and for the bimetallic catalyst a maximum conversion of 62% is attained at 550 °C. The initial conversion of W-Fe-Cu-Zag was about 20% over the whole temperature range; the conversion profile rose monotonically, reaching a maximum conversion of more than 70% at 490 °C and remained stable until the end of the catalytic test, excluding any deactivation caused by the phenomenon of ammonia oxidation.

Over the entire temperature range, all supports were N₂ selective, with selectivities surpassing 90% (Figure 11a). In the case of Fe-Cu-Zag, the production of N₂ has degraded to two minimums at around 350 °C and 450 °C. As seen in Figure 11b, this observation has been linked to an increase in the creation of the undesired nitrous oxide product. Fe-Cu-Zag has a tendency to generate N₂O at a high temperature (>400 °C) instead of decomposing NO in the presence of NH₃ according to the reaction path [43]:

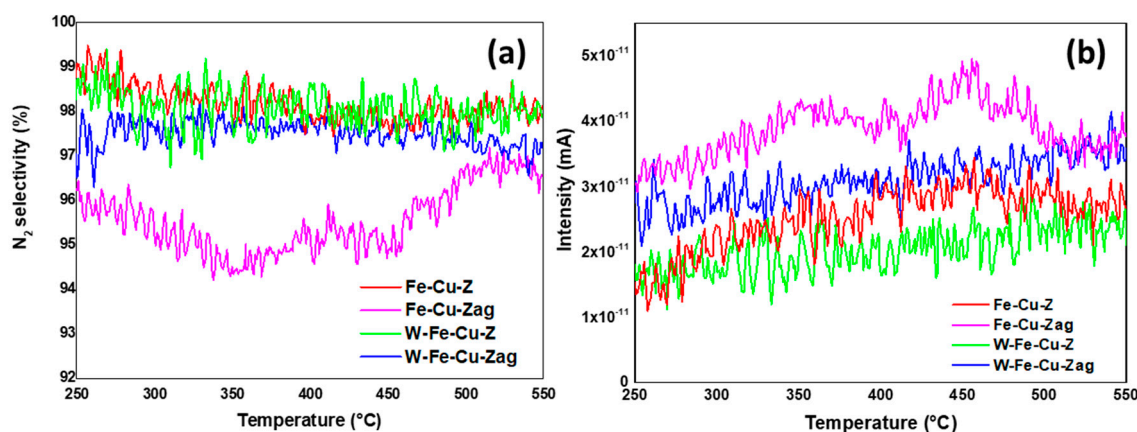


Figure 11. (a) N₂ selectivity and (b) Evolution of N₂O⁺ fragment (m/e = 44) intensity over studied catalysts.

For both fresh and steamed catalysts, the generation of N₂O was rather constant throughout the catalytic test but was less significant in the presence of W.

3. Discussion

The hydrothermal stability of the W-Fe-Cu-ZSM-5 catalyst for the ammonia selective catalytic reduction of NO has been investigated. Major findings and conclusions of this study are listed below:

- Iron and copper are known for their good ability to oxidize NO to NO₂, which is the rate-determining step of the standard NH₃-SCR reaction in the presence of O₂ [5,6]. The addition of tungsten into the fresh Fe-Cu-Z did not improve its low temperature catalytic activity at low temperatures probably due to the lack of acidity and/or redox active components. Furthermore, as detected using the UV-vis technique, a fresh Fe-Cu-Z catalyst encloses oligonuclear Fe³⁺_xO_y clusters, known as an active site for the NH₃-SCR of NO reaction [44]. The ameliorated activity of a fresh W-based catalyst above 450 °C may be ascribed to the presence of a tetrahedrally W(VI) species known as an active site for SCR process [11]. W-O-Si and W-O-Al active sites are the two main types of W species on W-ZSM-5, according to Chen et al. [11]. The presence of the tetrahedral W-O-Al structure was proved using ²⁷Al NMR on a W-Fe-Cu-Z sample.

- The aging process considerably deteriorated the NO conversion over the Fe-Cu-Z catalyst; however, this sample showed a better acidity compared to the trimetallic sample above 400 °C. This explains its best starting activity, which dropped to zero as Cu atoms were displaced from their counter-cation locations in the support and formed CuAl₂O₄ and CuO aggregates detected mainly owing to STEM and H₂-TPR techniques, which is in line with our previous study that also draws attention to copper oxide production following high-temperature aging for an Fe-Cu-ZSM-5 system [45]. These agglomerates are responsible for catalytic deactivation and are known to be very active for high temperature NO oxidation, as well NH₃ oxidation, with a high selectivity in nitrogen oxide formation [46,47].
- This research points out that the stability of the tungsten-based catalyst at low reaction temperatures against hydrothermal treatment is attributed to its good redox properties as demonstrated from H₂-TPR. Since the reducibility of the metal ions controls the extent of low temperature NO conversion in metal exchanged zeolite catalysts, the easier the reduction of metal species, the higher their oxidation ability in the SCR process [48].
- Our results suggest that the studied samples reached the “severe” stage of aging (observed between 750 and 850 °C) as described by Luo et al. [46]. This scenario shows no structural breakdown of the zeolite and is accompanied by an agglomeration of the metal atoms and a lowering of Brönsted acid sites, leading to low temperature NH₃ storage and NO conversion, which is in accordance with the findings of our study. In the case of W-Fe-Cu-Zag, the agglomeration of W and Fe as seen from EDX mapping images was beneficial to its catalytic stability. According to earlier research, adding surface tungsten oxide to SCR catalysts increases their reactivity while also having an inhibitory influence on the generation of unwanted N₂O during the reaction process [49,50].

4. Materials and Methods

4.1. Catalysts Preparation

The desired materials with the theoretical composition specified in Table 1 were prepared using solid-state ion exchange (SSIE) following the consecutive steps cited below:

Step 1: 1 g of commercial NH₄⁺-ZSM-5 (Si/Al = 15) furnished by Zeolyst International (CBV3024E) was mixed and finely ground in an agate mortar with the desired amount of the precursor CuCl₂ · 2H₂O (Sigma-Aldrich, St. Louis, MO, USA) under ambient conditions for 5 min. The obtained mixture was then treated for 12 h at 380 °C under a stream of He (Air Liquide, 99.99%) using a flow rate of 30 cm³ min⁻¹ and a heating rate of 2 °C min⁻¹.

Step 2: The powder resulting from the first step was in turn mixed and finely ground, under the same conditions cited in “step 1”, with the desired amount of the precursor FeCl₂ · 4H₂O (Sigma-Aldrich, Missouri, USA), then heated at 290 °C during 12 h in He steam. The final material was labelled Fe-Cu-Z.

Step 3: WO₃/Fe-Cu-ZSM-5 catalyst (labeled as W-Fe-Cu-Z) was prepared by mixing 1 g of Fe-Cu-Z solid with the desired amount of the precursor (NH₄)₆H₂W₁₂O₄₀ · xH₂O Sigma-Aldrich, Missouri, USA) through mechanical grinding in an agate mortar. The resulting mixture was ultimately treated in a steam of He during 12 h at 500 °C using a flow rate of 30 cm³ min⁻¹ and a heating rate of 1 °C min⁻¹.

4.2. Catalysts Aging

The aging process was carried out as follows: 200 mg of catalyst were placed on the porous frit of a U-tube quartz reactor that circulates a gas flow (20% O₂/He) at a flow rate of 50 cm³ min⁻¹. The reactor was then heated with a gradient of 6 °C min⁻¹ to 850 °C. Starting at this temperature, a syringe pump began injecting H₂O (liq.) at a flow rate of 0.0041 cm³ min⁻¹ for 5 h. The oven was eventually cooled to room temperature and once the temperature reaches 450 °C, the H₂O injection was stopped. The steamed catalysts were labelled Fe-Cu-Zag and W-Fe-Cu-Zag.

4.3. Physical and Chemical Characterization

The chemical analysis of the prepared samples was performed using ICP-OES with a Varian 715-ES spectrometer with a wavelength coverage of 177–785 nm. Textural properties were investigated using N₂-physisorption at 77 K technique with the aid of Micromeritics ASAP 2000 equipment. Previously, the samples were degassed at 250 °C for 5 h. The samples' morphology was checked using Field Emission Scanning Electron Microscopy with a ZEISS ULTRA-55 microscope working at an accelerating voltage of 20 keV in analysis mode. The sample powder was deposited in double-sided tape and analyzed using carbon covering. The sample coating was performed with a BAL-TEC SCD005 instrument. The solid-state MAS NMR analyses were conducted on a Bruker AV400 spectrometer at room temperature. ²⁷Al and ²⁹Si measurements were referred to as Al(NO₃)₃ (0.1M) and TMS, respectively. The ²⁹Si MAS NMR spectra were recorded using a BL-7 probe with 7 mm diameter zirconia rotors spinning at 5 kHz using a recycle delay of 3 s. The ²⁷Al MAS NMR were recorded using a BL4mm probe with 4mm diameter zirconia rotors spinning at 14 kHz using a recycle delay of 1 s and pulses of $\pi/12$. Employing a PANalytical Cubix'Pro diffractometer with an X' Celerator detector and automatic divergence and reception slits using Cu-K radiation, the samples' crystallinity was examined (0.154056 nm). The instrument was powered by a 45 kV voltage and a 40 mA current. The software PANalytical X' Pert HighScore Plus was used to analyze the diffractograms, which were recorded in the range of 5–40°. The DRS UV-vis experiments were carried out using a Cary 7000 spectrometer equipped with a diffuse reflectance accessory (Praying Mantis Harrick). Using BaSO₄ as an internal standard, the spectra were obtained at room temperature in the 200–800 nm wavelength range. STEM micrographs and EDX mapping analysis were carried out using a JEOL-JEM 2100F instrument equipped with an X-MAX microanalysis detector and operating under a resolution energy of 20 eV and an accelerating voltage of 200 kV. The samples were suspended in a volume of isopropanol and subjected to an ultrasonic bath for 20 min and a drop of this solution was deposited on a nickel grid. The H₂-TPR profiles were obtained on an automated Micromeritics Autochem 2920 instrument. Previously, 50 mg of each sample was pretreated at 500 °C (10 °C min⁻¹) under 5%O₂/He atmosphere (30 cm³ min⁻¹) in a quartz U-tube reactor for 30 min and then cooled under He to 40 °C. The H₂-TPR measurements were performed under 5%H₂/Ar flow (30 cm³ min⁻¹) in the temperature range 40–800 °C (5 °C min⁻¹). The acid properties of the catalysts were determined using FTIR spectroscopy of adsorbed pyridine (FTIR-Pyr) with the aid of Nicolet 710 FTIR equipment. Before spectra recording, 13 mg of catalysts were pressed into sheets and degassed overnight at 400 °C under dynamic vacuum (10⁻⁶ mbar). Pyridine was adsorbed until equilibration after cooling to room temperature and then the samples were degassed at different temperatures (150 °C, 250 °C, 350 °C, and 400 °C) and following each desorption step, the corresponding spectrum was recorded.

4.4. Catalytic Tests

The NH₃-SCR of NO catalytic tests were carried out in a temperature programmed surface reaction (TPSR) with the aid of a flow reactor operating at atmospheric pressure with a total flow rate of 6 L h⁻¹ and a space velocity of 333.333 h⁻¹. A sample amount of 18 mg was activated in situ under an O₂ and He mixture (8% O₂, 88.3% He and 3.5% H₂O) at 250 °C and then cooled to 50 °C. The catalysts were tested in the temperature range 250–550 °C, with a ramp of 3.75 °C min⁻¹, under the same atmosphere used for their activation and using the following gas composition: 1000 ppm of NH₃ and 1000 ppm of NO. The gas mixture of the studied reaction was administrated to the reactor using mass flow controllers. The effluent composition was continuously monitored and by sampling on line to an Omnistar Pfeiffer Vacuum quadruple mass spectrometer equipped with both Faraday and Channeltron detectors. Results gathered from catalytic tests were expressed as follows:

$$X_{\text{NO}} = \frac{[\text{NO}_0] - [\text{NO}_T]}{[\text{NO}_0]} \times 100$$

where $[\text{NO}_T]$ and $[\text{NO}_0]$ account for the NO concentrations at the temperature T and at the inlet gas reactor, respectively.

5. Conclusions

Fresh Fe-Cu-ZSM-5 and $\text{WO}_3/\text{Fe-Cu-ZSM-5}$ SCR catalysts were hydrothermally treated in the presence of 10% water vapor at 850 °C for 5 h in a U-tube quartz reactor. The aging of the catalysts influenced the structural, textural, and metal speciation of the studied catalysts: the Fe-Cu-ZSM-5 catalyst undergoes extensive deterioration of its NH_3 -SCR activity after hydrothermal treatment at 850 °C. CuO and CuAl_2O_4 formation is majorly responsible for the loss of activity occurring both at 300 °C and at high temperature. Tungsten deposition onto Fe-Cu-ZSM-5 does not modify in a meaningful way the catalytic performance of the host catalyst. After the aging of $\text{WO}_3/\text{Fe-Cu-ZSM-5}$, the NH_3 -SCR activity of NO also deteriorated, but the presence of tungsten oxide crystallites and iron oligonuclear clusters, both known as active species for the NH_3 -SCR reaction, allowed a better stability of the aged catalyst at low temperatures and specially improved its activity at high temperatures.

Supplementary Materials: The following supporting information can be downloaded at: <https://www.mdpi.com/article/10.3390/inorganics10110180/s1>, Figure S1. EDX reports of analyzed spectra recorded on (a) Fe-Cu-Z, (b) Fe-Cu-Zag, (c) W-Fe-Cu-Z, and (d) W-Fe-Cu-Zag catalysts.

Author Contributions: Project administration, I.M. and M.M.; Catalysts preparation, H.J. and R.B.; NH_3 -SCR catalytic testing, H.J. and G.D.; UV-vis DRS and H_2 -TPR analysis performing, T.B.; XRD, FTIR-Pyr and MAS NMR analysis performing, A.d.M.-G.; writing—original draft preparation, H.J.; writing—review and editing, G.D. All authors have read and agreed to the published version of the manuscript.

Funding: This research received no external funding.

Acknowledgments: The authors thank the Microscopy Service of the Universitat Politècnica de València for its assistance in sample characterization. Teresa Blasco acknowledge the financial support of the Generalitat Valenciana, Conselleria d'Innovació, Universitats Ciència y Societat Digital (Prometeo/2021/077) and the Spanish Ministry of Science and Innovation (SEV-2016-0683-19-2). Alessandra de Marcos-Galán thanks the predoctoral grant PRE2019-090465.

Conflicts of Interest: The authors declare no conflict of interest.

References

1. Li, J.; Chang, H.; Ma, L.; Hao, J.; Yang, R.T. Low-temperature selective catalytic reduction of NO_x with NH_3 over metal oxide and zeolite catalysts—A review. *Catal. Today* **2011**, *175*, 147–156. [CrossRef]
2. Brandenberger, S.; Kröcher, O.; Tissler, A.; Althoff, R. The State of the Art in Selective Catalytic Reduction of NO_x by Ammonia Using Metal-Exchanged Zeolite Catalysts. *Catal. Rev. Sci. Eng.* **2008**, *50*, 492–531. [CrossRef]
3. Kanazawa, T. MFI zeolite as a support for automotive catalysts with reduced Pt sintering. *Appl. Catal. B* **2006**, *65*, 185–190. [CrossRef]
4. Bi, Y.; Chen, L.; Lu, G. Constructing surface active centres using Pd–Fe–O on zeolite for CO oxidation. *J. Mol. Catal. A* **2007**, *266*, 173–179. [CrossRef]
5. Jouini, H.; Mejri, I.; Petitto, C.; Martinez-Ortigosa, J.; Vidal-Moya, A.; Mhamdi, M.; Blasco, T.; Delahay, G. Characterization and NH_3 -SCR reactivity of Cu-Fe-ZSM-5 catalysts prepared by solid state ion exchange: The metal exchange order effect. *Microporous Mesoporous Mat.* **2018**, *260*, 217–226. [CrossRef]
6. Jouini, H.; Mejri, I.; Martinez-Ortigosa, J.; Cerrillo, J.L.; Mhamdi, M.; Palomares, A.E.; Delahay, G.; Blasco, T. Selective catalytic reduction of nitric oxide with ammonia over Fe-Cu modified highly silicated zeolites. *Solid State Sci.* **2018**, *84*, 75–85. [CrossRef]
7. Jouini, H.; Martinez-Ortigosa, J.; Mejri, I.; Mhamdi, M.; Blasco, T.; Delahay, G. On the performance of Fe-Cu-ZSM-5 catalyst for the selective catalytic reduction of NO with NH_3 : The influence of preparation method. *Res. Chem. Intermed.* **2019**, *45*, 1057–1072. [CrossRef]
8. Jouini, H.; Mejri, I.; Martinez-Ortigosa, J.; Cerrillo, J.L.; Petitto, C.; Mhamdi, M.; Blasco, T.; Delahay, G. Alkali poisoning of Fe-Cu-ZSM-5 catalyst for the selective catalytic reduction of NO with NH_3 . *Res. Chem. Intermed.* **2022**, *48*, 3415–3428. [CrossRef]
9. Wu, T.; Li, S.; Yuan, G.; Zhao, D.; Chen, S.; Xu, J.; Hua, T. Enhanced selectivity of propylene in butylene catalytic cracking over W-ZSM-5. *Fuel Process Technol.* **2018**, *173*, 143–152. [CrossRef]

10. Zhu, Z.; Lu, G.; Guo, Y.; Guo, Y.; Zhang, Z.; Wang, Y.; Gong, X.-Q. High Performance and Stability of the Pt-W/ZSM-5 Catalyst for the Total Oxidation of Propane: The Role of Tungsten. *Chem. Cat. Chem.* **2013**, *5*, 2495–2503. [[CrossRef](#)]
11. Chen, J.; Yan, H.; Gong, H.; Zhang, H.; Zhou, Y.; Gao, C.; Liu, Y.; Chen, X.; Yang, C. Tetrahedrally coordinated W(VI) species induced Lewis acid for stable catalytic cracking of 1-hexene to propene. *Chem. Eng. J.* **2022**, *448*, 137504. [[CrossRef](#)]
12. Wang, X.; Zhang, S.; Yu, Q.; Yang, H. Tungsten promoted HZSM-5 in the SCR of NO by acetylene. *Microporous Mesoporous Mater.* **2008**, *109*, 298–304. [[CrossRef](#)]
13. Liu, H.; You, C.; Wang, H. Experimental and Density Functional Theory Studies on the Zeolite-Based Fe–Ni–W Trimetallic Catalyst for High-Temperature NO_x Selective Catalytic Reduction: Identification of Active Sites Suppressing Ammonia Over-oxidation. *ACS Catal.* **2021**, *11*, 1189–1201. [[CrossRef](#)]
14. Mohan, S.; Dinesha, P.; Kumar, S. NO_x reduction behaviour in copper zeolite catalysts for ammonia SCR systems: A review. *Chem. Eng. J.* **2019**, 123253. [[CrossRef](#)]
15. Yuanqing, Z.; Weihao, Z.; Chong, X.; Qichen, H. Application and Development of Selective Catalytic Reduction Technology for Marine Low-Speed Diesel Engine: Trade-Off among High Sulfur Fuel, High Thermal Efficiency, and Low Pollution Emission. *Atmosphere* **2022**, *13*, 731.
16. Thommes, M.; Kaneko, K.; Neimark, A.V.; Olivier, J.P.; Rodriguez-Reinoso, F.; Rouquerol, J.; Sing, K.S.W. Physisorption of gases, with special reference to the evaluation of surface area and pore size distribution (IUPAC Technical Report). *Pure Appl. Chem.* **2015**, *78*, 1051–1069. [[CrossRef](#)]
17. Abid, R.; Delahay, G.; Tounsi, H. Selective catalytic reduction of NO by NH₃ on cerium modified faujasite zeolite prepared from aluminum scraps and industrial metasilicate. *J. Rare Earths* **2019**, *38*, 250–256. [[CrossRef](#)]
18. Wang, L.-C.; Zhang, Y.; Xu, J.; Diao, W.; Karakalos, S.; Liu, B.; Song, X.; Wu, W.; He, T.; Ding, D. Non-oxidative dehydrogenation of ethane to ethylene over ZSM-5 zeolite supported iron catalysts. *Appl. Catal.* **2019**, *256*, 117816. [[CrossRef](#)]
19. Iwasaki, M.; Yamazaki, K.; Banno, K.; Shinjoh, H. Characterization of Fe/ZSM-5 DeNO_x catalysts prepared by different methods: Relationships between active Fe sites and NH₃-SCR performance. *J. Catal.* **2008**, *260*, 205–216. [[CrossRef](#)]
20. Hongrutai, N.; Watmanee, S.; Wannakao, S.; Praserttham, P.; Panpranot, J. Effect of small amounts of Al on the surface silanol structure and their correlation to the improved catalytic performances of WO_x/SiO₂–Al₂O₃ in the propene self-metathesis. *Mater. Today Chem.* **2021**, *21*, 100492. [[CrossRef](#)]
21. Wan, C.; Hu, M.Y.; Jaegers, N.R.; Shi, D.; Wang, H.; Gao, F.; Qin, Z.; Wang, Y.; Hu, J.Z. Investigating the Surface Structure of γ -Al₂O₃ Supported WO_x Catalysts by High Field ²⁷Al MAS NMR and Electronic Structure Calculations. *J. Phys. Chem. C* **2016**, *120*, 23093–23103. [[CrossRef](#)]
22. Zhang, Y.; Zhou, Y.; Yang, K.; Li, Y.; Wang, Y.; Xu, Y.; Wu, P. Effect of hydrothermal treatment on catalytic properties of PtSnNa/ZSM-5 catalyst for propane dehydrogenation. *Microporous Mesoporous Mater.* **2006**, *96*, 245–254. [[CrossRef](#)]
23. Kuehl, G.H.; Timken, H.K.C. Acid sites in zeolite Beta: Effects of ammonium exchange and steaming. *Microporous Mesoporous Mater.* **2005**, *21*, 35–36. [[CrossRef](#)]
24. Rhimi, B.; Mhamdi, M.; Kalevaru, V.N.; Martin, A. Synergy between vanadium and molybdenum in bimetallic ZSM-5 supported catalysts for ethylene ammoxidation. *RSC Adv.* **2016**, *6*, 65866–65878. [[CrossRef](#)]
25. Engelhardt, G.; Lohse, U.; Samoson, A.; Mägi, M.; Tarmak, M.; Lippmaa, E. High resolution ²⁹Si n.m.r. of dealuminated and ultrastable Y-zeolites. *Zolites* **1982**, *2*, 59–62. [[CrossRef](#)]
26. Ismagilov, Z.R.; Yashnik, S.A.; Anufrienko, V.F.; Larina, T.V.; Vasenin, N.T.; Bulgakov, N.N.; Vosel, S.V.; Tsykoza, L.T. Linear nanoscale clusters of CuO in Cu-ZSM-5 catalysts. *Appl. Surf. Sci.* **2004**, *226*, 88–93. [[CrossRef](#)]
27. Wilken, N.; Nedyalkova, R.; Kamasamudram, K.; Li, J.; Currier, N.W.; Vedaiyan, R.; Yezerets, A.; Olsson, L. Investigation of the Effect of Accelerated Hydrothermal Aging on the Cu Sites in a Cu-BEA Catalyst for NH₃-SCR Applications. *Top. Catal.* **2013**, *56*, 317–322. [[CrossRef](#)]
28. Gutiérrez-Alejandre, A.; Ramírez, J.; Busca, G. The electronic structure of oxide-supported tungsten oxide catalysts as studied by UV spectroscopy. *Catal. Lett.* **1998**, *56*, 29–33. [[CrossRef](#)]
29. Ramanathan, A.; Subramaniam, B.; Badloe, D.; Hanefeld, U.; Maheswari, R. Direct incorporation of tungsten into ultra-large-pore three-dimensional mesoporous silicate framework: W-KIT-6. *J. Porous Mater.* **2012**, *19*, 961–968. [[CrossRef](#)]
30. Zhao, D.; Rodriguez, A.; Dimitrijevic, N.M.; Rajh, T.; Koodali, R.T. Comparative Influence of Surface Tungstate Species and Bulk Amorphous WO₃ Particles on the Acidity and Catalytic Activity of Tungsten Oxide Supported on Silica. *J. Phys. Chem. C* **2010**, *114*, 15728–15734. [[CrossRef](#)]
31. Chauvin, J.; Thomas, K.; Clet, G.; Houalla, M. Comparative Influence of Surface Tungstate Species and Bulk Amorphous WO₃ Particles on the Acidity and Catalytic Activity of Tungsten Oxide Supported on Silica. *J. Phys. Chem. C* **2015**, *119*, 12345–12355. [[CrossRef](#)]
32. Delahay, G.; Coq, B.; Broussous, L. Selective catalytic reduction of nitrogen monoxide by decane on copper-exchanged beta zeolites. *Appl. Catal. B Environ.* **1997**, *12*, 49–59. [[CrossRef](#)]
33. Delahay, G.; Guzmán-Vargas, A.; Valade, D.; Coq, B. Selective Catalytic Reduction of NO by NH₃ on Fe-ZSM-5 Elaborated from Different Methods. *Stud. Surf. Sci. Catal. C* **2004**, *154*, 2501–2508.
34. Kim, Y.J.; Lee, J.K.; Min, K.M.; Hong, S.B.; Nam, I.-S.; Cho, B.K. Hydrothermal stability of CuSSZ13 for reducing NO_x by NH₃. *J. Catal.* **2014**, *311*, 447–457. [[CrossRef](#)]

35. Cavataio, G.; Jen, H.-W.; Warner, J.R.; Girard, J.W.; Kim, J.Y.; Lambert, C.K. Enhanced Durability of a Cu/Zeolite Based SCR Catalyst. *SAE Int. J. Fuels Lubr.* **2008**, *1*, 477–487. [[CrossRef](#)]
36. Putluru, S.S.R.; Schill, L.; Jensen, A.D.; Fehrmann, R.S.N. Selective Catalytic Reduction of NO_x with NH₃ on Cu-, Fe-, and Mn-Zeolites Prepared by Impregnation: Comparison of Activity and Hydrothermal Stability. *J. Chem.* **2018**, *2018*, 1–11. [[CrossRef](#)]
37. de Lucas, A.; Valverde, J.L.; Rodriguez, L.; Sanchez, P.; Garcia, M.T. Modified W/HZSM-5 catalysts: Structure and catalytic properties. *J. Mol. Catal. A* **2001**, *171*, 195–203. [[CrossRef](#)]
38. Wang, C.; Yang, S.; Chang, H.; Peng, Y.; Li, J. Dispersion of tungsten oxide on SCR performance of V₂O₅ single bond WO₃/TiO₂: Acidity, surface species and catalytic activity. *Chem. Eng. J.* **2013**, *225*, 520–527. [[CrossRef](#)]
39. Bahmanpour, A.M.; Le Monnier, B.P.; Du, Y.-P.; Héroguel, F.; Luterbacher, J.S.; Kröcher, O. Increasing the activity of the Cu/CuAl₂O₄/Al₂O₃ catalyst for the RWGS through preserving the Cu²⁺ ions. *Chem. Comm.* **2021**, *57*, 1153–1156. [[CrossRef](#)]
40. Emeis, C.A. Determination of Integrated Molar Extinction Coefficients for Infrared Absorption Bands of Pyridine Adsorbed on Solid Acid Catalysts. *J. Catal.* **1993**, *141*, 347–354. [[CrossRef](#)]
41. Bhuiyan, T.I.; Arudra, P.; Akhtar, M.N.; Aitani, A.M.; Abudawoud, R.H.; Al-Yami, M.A.; Al-Khattaf, S.S. Metathesis of 2-butene to propylene over W-mesoporous molecular sieves: A comparative study between tungsten containing MCM-41 and SBA-15. *Appl. Catal. A Gen.* **2013**, *467*, 224–234. [[CrossRef](#)]
42. Väliheikki, A.; Kolli, T.; Huuhtanen, M.; Maunula, T.; Kinnunen, T.; Keiski, R.L. The Effect of Biofuel Originated Potassium and Sodium on the NH₃-SCR Activity of Fe-ZSM-5 and W-ZSM-5 Catalysts. *Top. Catal.* **2013**, *56*, 602–610. [[CrossRef](#)]
43. Madia, G.; Koebel, M.; Elsener, M.; Wokaun, A. Side Reactions in the Selective Catalytic Reduction of NO_x with Various NO₂ Fractions. *Ind. Eng. Chem. Res.* **2002**, *41*, 4008–4015. [[CrossRef](#)]
44. Heinrich, F.; Schmidt, C.; Löffler, E.; Menzel, M.; Grünert, W. Fe-ZSM-5 Catalysts for the Selective Reduction of NO by Isobutane—The Problem of the Active Sites. *J. Catal.* **2002**, *212*, 157–172. [[CrossRef](#)]
45. Jouini, H.; Mejri, I.; Rhimi, B.; Mhamdi, M.; Blasco, T.; Delahay, G. Ce-promoted Fe-Cu-ZSM-5 catalyst: SCR-NO activity and hydrothermal stability. *Res. Chem. Intermed.* **2021**, *47*, 2901–2915. [[CrossRef](#)]
46. Luo, J.; An, H.; Kamasamudram, K.; Currier, N.; Yezerets, A.; Watkins, T.; Allard, L. Impact of Accelerated Hydrothermal Aging on Structure and Performance of Cu-SSZ-13 SCR Catalysts. *SAE Int. J. Eng.* **2015**, *8*, 1181–1186. [[CrossRef](#)]
47. Zheng, W.; Chen, J.; Guo, L.; Zhang, W.; Zhao, H.; Wu, X. Research progress of hydrothermal stability of metal-based zeolite catalysts in NH₃-SCR reaction. *J. Fuel Chem. Technol.* **2020**, *48*, 1193–1207. [[CrossRef](#)]
48. Arakawa, K.; Matsuda, S.; Kinoshita, H. SO_x poisoning mechanism of NO_x selective reduction catalysts. *Appl. Surf. Sci.* **1997**, *121–122*, 382–386. [[CrossRef](#)]
49. Jaegers, N.R.; Lai, J.-K.; He, Y.; Walter, E.; Dixon, D.A.; Vasiliu, M.; Chen, Y.; Wang, C.; Hu, M.Y.; Mueller, K.T.; et al. Mechanism by which Tungsten Oxide Promotes the Activity of Supported V₂O₅/TiO₂ Catalysts for NO_x Abatement: Structural Effects Revealed by ⁵¹V MAS NMR Spectroscopy. *Angew. Chem.* **2019**, *131*, 12739–12746. [[CrossRef](#)]
50. Ye, D.; Qu, R.; Song, H.; Zheng, C.; Gao, X.; Luo, Z.; Ni, M.; Cen, K. Investigation of the promotion effect of WO₃ on the decomposition and reactivity of NH₄HSO₄ with NO on V₂O₅-WO₃/TiO₂ SCR catalysts. *RSC Adv.* **2016**, *6*, 55584–55592. [[CrossRef](#)]